International Journal of Innovative Technology and Exploring Engineering (IJITEE)
ISSN: 2278-3075 (Online), Volume-9 Issue-4, February 2020

An Elasto-Plastic Ball Bearing Contact with Bilinear Hardening

Leong Chee Yau, Wan Fathul Hakim W. Zamri, Intan Fadhlina Mohamed, Ahmad Kamal Ariffin, Muhammad Faiz Md Din

Abstract: ***This study is an analytical evaluation of contact and wear on ball bearings using the finite element method. Ball bearings are used in various sectors, such as in the automobile, turbine and aircraft engine industries, to reduce rotational friction and support radial loads. Nevertheless, ball bearings often experience failure due to wear as a consequence of contact pressure. The contact between the ball bearing components will affect the surface of the balls, and the inner and outer rings. Therefore, the main objective of this study was to examine the stress distribution and elasto-plastic deformation in order to analyse the contact between the ball bearing components. Most of the existing contact and wear models for ball bearings only take into account the elastic model. However, an analytical evaluation of contact and wear using an elastic model, while ignoring plastic deformation, is inaccurate. In this study, a contact analysis was performed using elasto-plastic models of a ball bearing, and the results were validated using data from a previous research. Boundary loads of between 100 N to 800 N were applied and plasticity values of 550 MPa, 1050 MPa, 1550 MPa and 2050 MPa were used to analyse the contact behaviour. As the boundary load increased, the maximum contact pressure and displacement of the ball bearing increased. As the plasticity, E_2 rose higher, the maximum plastic strain was lowered proportionally.***

Keywords: ***Ball bearings, Contact, Elasto-plastic, Finite element method.***

I. INTRODUCTION

Ball bearing is a critical component in a system that can reduce the rotational friction and support radial load as well as axial load. Ball bearing is used to ensure the transmission of rotational motion with lowest friction.

Revised Manuscript Received on February 28, 2020.
***** Correspondence Author
Leong Chee Yau*, Department of Mechanical and Manufacturing Engineering, Faculty of Engineering and Built Environment, Universiti Kebangsaan Malaysia, Bangi, Malaysia. E-mail: cheeyau_95@hotmail.com
Wan Fathul Hakim W. Zamri*, Department of Mechanical and Manufacturing Engineering, Faculty of Engineering and Built Environment, Universiti Kebangsaan Malaysia, Bangi, Malaysia. E-mail: wfathul.hakim@ukm.edu.my
Muhammad Faiz Md Din, Department of Electrical & Electronics, Faculty of Engineering, Universiti Pertahanan Nasional Malaysia, Kuala Lumpur, Malaysia. E-mail: faizmd@upnm.edu.my
Intan Fadhlina Mohamed, Department of Mechanical and Manufacturing Engineering, Faculty of Engineering and Built Environment, Universiti Kebangsaan Malaysia, Bangi, Malaysia. E-mail: intanfadhlina@ukm.edu.my
Ahmad Kamal Ariffin, Department of Mechanical and Manufacturing Engineering, Faculty of Engineering and Built Environment, Universiti Kebangsaan Malaysia, Bangi, Malaysia. E-mail: kamal3@ukm.edu.my

Besides, it is often used in various sectors like electric motor, engine, aircraft, and conveyor as a connection which has low friction between rotating components [9]. Ball bearing has three main components that are ball, inner ring and outer ring as shown in Fig. 1. The type of ball bearing used in this study is 6309 DGBB which is widely used in conveyors. Nowadays, the ball bearing has been optimized to transmit more and more power with decreasing dimensions. The contact surfaces between contacting pairs become smaller and the contact pressure increases. The high contact pressure threatens the bearing materials which results in spalling of material [5]. The cost of replacing new rolling bearings is around $50.5 billion worldwide and will increase in the next decade. The study of contact stress at ball bearing will definitely contribute to the world in solving a lot of contact problem [2]. Ball bearing experiences contact stress at inner ring and outer ring. The damage of contacting surfaces and spalling of material are difficult to predict correctly. Besides, the contact stress and deformation at ball bearing cannot be obtained through experiment. The finite element simulation can be used to obtain the contact stress and deformation at the ball bearing [11]. A number of journals have been studied in to order to carry out a research that can contribute to the society. Researches about contact behavior on ball bearing have carried out by many researchers. In previous studies, Tang et al. 2011 [16], Guo et al. 2012 [4] and S. Li 2018 [6] have conducted contact simulation by using full geometry of ball bearing. The simulations focused on the contact between ball, inner ring, and outer ring. Tang et al. 2011 have studied the stress distribution at ball and inner ring of a ball bearing. Besides, Guo et al. 2012 [4] also used a full geometry of ball bearing but only focused on the ball component while S. Li 2018 [6] studied the stress distribution of the full geometry. Yang et al. 2016 [21] also have studied the contact simulation at ball bearing by using full geometry. The simulation focused on the inner ring and outer ring of the ball bearing. All these simulations have been carried out with only considering the elastic property of the material. A full geometry of ball bearing simulation takes a longer time compared to a simulation that uses a portion of the ball bearing geometry. Contact simulations focusing on the ball and inner ring were carried out by Shan et al. 2009 [12], Shan et al. 2009 [13], Zhou et al. 2011 [26], Londhe et al. 2018 [7], and Wang et al. 2011 [20]. The simulations of contact between ball and inner ring were often carried out because failure and spalling of material normally happen at the ball and inner ring.

The contact simulation between ball and inner ring that only used a portion of a full geometry of ball bearing and this used less time to carry out the simulation but all the simulations were carried out by using elastic model. Most of the studies on contact analysis only used the elastic model and only a few studies by Massi et al. 2014 [8], Tonnazi et al. 2017 [17] and Viellard et al. 2016 [18] used the elasto-plastic model to carry out a simulation at ball bearing. The aforementioned studies used elasto-plastic model for wear simulation but not contact simulation. Therefore, only a few number of researches that studied about the contact behavior on ball bearing with considering the plasticity of the material.

This study was carried out by using elasto-plastic model to study contact behavior on ball bearing with consideration of both elastic and plastic behavior of bearing material. The objectives of this research were to examine the stress distribution and effect of elasto-plastic deformation for contact analysis at ball bearing.

Fig. 1.Structure of a ball bearing [9].

II. LINEAR AND NONLINEAR CONTACT MODEL

An understanding of contact simulation between the ball and inner ring begins with a study of contact mechanics between two solids. The theory that can help researcher in understanding the contact mechanisms in a ball bearing is Hertz theory. The Hertz theory was introduced by Hertz in 1895 which is a linear contact model and also widely used to solve contact problem between two objects. Linear contact model is valid in a model with linear stress-strain relationship without exceeds the yield stress limit. In reality, the contacts between two or more objects result a dramatically change in stress and strain which is a nonlinear contact. The structures with behaviors of large plastic deformations, viscoelastic properties, time-dependent fatigue and failure progression can be considered as nonlinear contact model. These behaviors are difficult to be analyzed by using linear contact model due to the nonlinear relationship of stress-strain [19]. The contact area dimension is also one of the main criteria that can be obtained through Hertz theory [10]. Several assumptions of this theory are (i) the two contacting objects must be homogeneous and isotropic, (ii) applied load must be perpendicular to the contact surface, (iii) object can only have elastic deformation and (iv) contact surface size is small compared to the contact surface of radius of curvature [22]. Fig. 2 shows a contact of sphere on a plate. The sphere represents the ball while the plate represents the inner ring in the simulation. The reduced radius of curvature, $R^{'}$ of the contact model can be calculated by:

$$\frac{1}{R^{'}} = \frac{1}{R_x} + \frac{1}{R_y} \tag{1}$$

where R_x is the radius of sphere and plate at x- axis and R_y is the radius of sphere and plate at y- axis. The reduced Young's modulus, $E^{'}$ is then calculated by:

$$\frac{1}{E^{'}} = \frac{1}{2}\left[\frac{1-v_A^2}{E_A} + \frac{1-v_B^2}{E_B}\right] \tag{2}$$

where v_A is the Poisson's ration of ball while v_B is the Poisson's ratio of the inner ring. The E_A and E_B are the Young's modulus of ball and inner ring material. The contact area dimension, a of the ball at sphere is written as:

$$a = \left(\frac{3WR^{'}}{E^{'}}\right)^{\frac{1}{3}} \tag{3}$$

W is the load applied. The maximum contact pressure can be calculated by using the contact area dimension, a that obtained from (3). The maximum contact pressure, P_{max} can be written as:

$$P_{\max} = \frac{3W}{2\pi a^2} \tag{4}$$

The maximum contact pressure at the ball bearing can be calculated by using (4) when the load applied and contact area dimension are known [15].

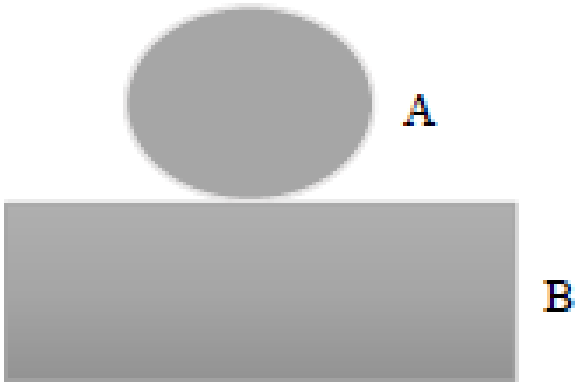

Fig. 2.Contact between sphere and plate.

III. FINITE ELEMENT ANALYSIS AND MODEL DESCRIPTION

Contact simulations were performed to study the stress distribution at ball bearing by using ABAQUS finite element software. The contact analysis schematic diagram is shown in Fig. 3. The boundary load,

F was applied at the ball to obtain the stress distribution. The explicit finite element simulation was carried out for the contact simulation. Diameter of the ball was 12.7 mm while the length and width of the inner ring were 12 mm and 3 mm as shown in Table I. The material used for the ball bearing was bearing steel with Young's modulus 200 GPa, Poisson ratio of 0.3 and density of 7.90 g/cm^3. The material property of the model is shown in Table II. The interaction property between the ball and inner ring was surface-to-surface. The simulation time for the contact analysis was 0.13 s. The bottom surface of the inner ring was fixed for all direction of motion and the ball surface is fixed for X direction and rotation. The boundary load was applied at the top surface of the ball. The mesh of the 2 dimensional model is shown in Fig. 4. The high number of element was located at the contact region of the ball bearing. This is to ensure the accuracy of the result and reduce the simulation time. The number of element for the contact analysis was 9522 and the element type used was CPE4R and plane strain.

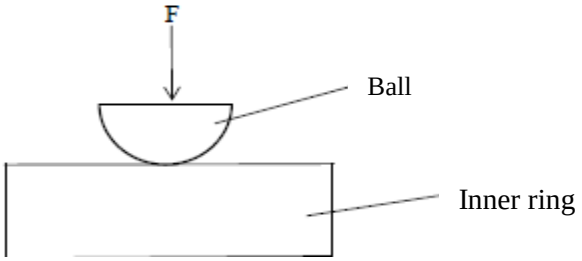

Fig. 3.Schematic diagram of contact analysis of ball bearing.

Table-I: Geometry parameter of contact model [7], [14]

Diameter of ball	12.7 mm
Inner ring	12 mm × 3 mm

Table-II: Material properties of inner ring and ball [7]

Material	Young's Modulus (GPa)	Poisson's Ratio	Density (g/cm^3)
Steel bearing (GCr15)	200	0.3	7.90

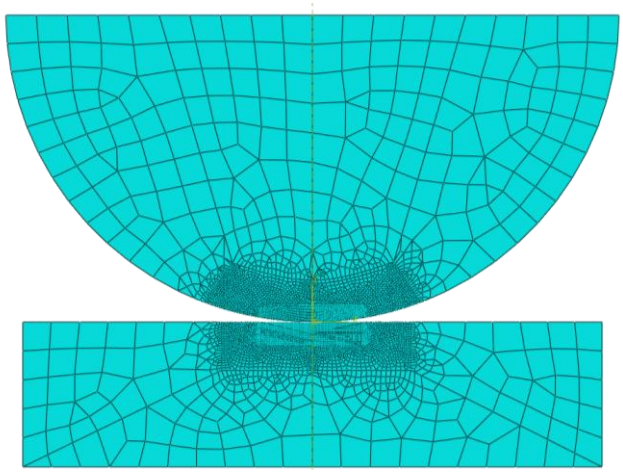

Fig. 4.Mesh of contact analysis.

IV. RESULT AND DISCUSSION

A. Model Verification

The finite element model used has been carried out a convergence study. The convergence study of meshing converge was done to obtain more accurate results. The initial meshing had an element number of 314 and the maximum contact pressure that was obtained from simulation was 508 MPa when the applied load was 100 N. The finite element model started to converge when the number of element was 4340 with a consistent maximum contact pressure of 1750 MPa. The Fig. 5 shows the graph of the maximum contact pressure versus the number of element. The amplitude of the load applied was 55. This was to ensure the speed of the load applied was same as the real case of contact at ball bearing. The amplitude between any two consecutive data points, a^* can be calculated by:

$$a^* = A_i + (A_{i+1} - A_i)T^3(10 - 15T + 6T^2) \quad (5)$$

where A_i is the first data, A_{i+1} is the second data and T is given by:

$$T = \frac{t - t_i}{t_{i+1} - t_i} \quad (6)$$

where t is total time, t_i is the first time data and t_{i+1} is the second time data. An amplitude is a differentiation of a^* with respect to T that can be obtained as follows:

$$\frac{\partial a^*}{\partial T} = (30A_{i+1} - 20A_i)T^2 + (-20A_{i+1} + 15A_i)T^3 + (30A_{i+1} - 24A_i)T^4 \quad (7)$$

The amplitude of the applied load can be obtained by using (7) [1]. The high amplitude of applied load means the applied load speed is high. The maximum contact pressure obtained through the contact simulation was 1751 MPa while the maximum contact pressure obtained from the other journal was 1785 MPa. The difference in percentage was 1.90 %. The maximum contact pressure obtained through analytic calculation was 1800 MPa and the difference in percentage between analytic calculation and simulation was 2.72 %. It was confirmed that this model is accurate and can be used for related studies as the percentage differences were lower than 5%. Therefore, the model was validated and can be used to carry out other simulation. Table III shows the comparison of the maximum contact pressure obtained from finite element simulation, journal, and analytic calculation. Fig. 6 shows the stress contour of the contact simulation with 100 N boundary load applied.

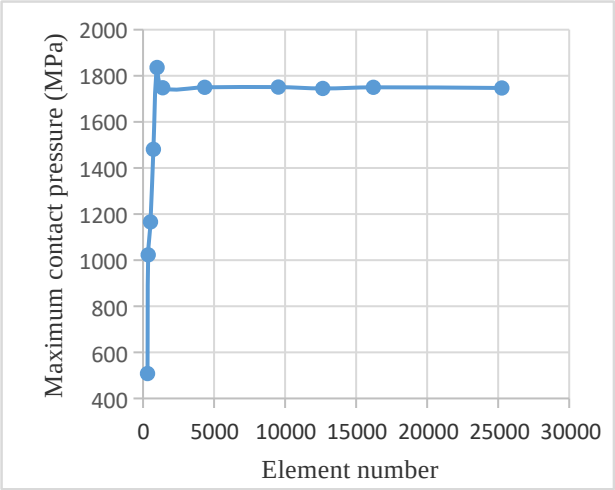

Fig .5.Graph of Maximum contact pressure vs. Element number.

Table-III: Comparison of simulation results with journal values

Maximum contact pressure		
Results of simulation	Journal results of simulations [7]	Analytical Calculations
1751 MPa	1785 MPa	1800 MPa
Percentage Difference	1.90 %	2.72 %

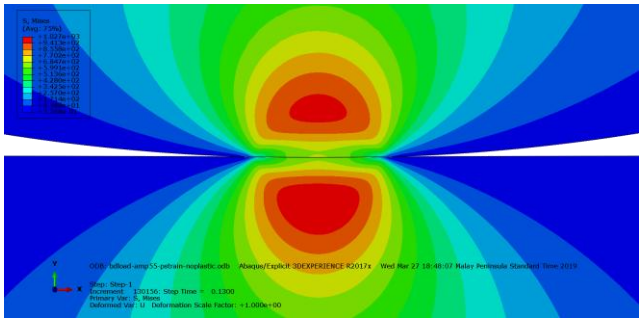

Fig. 6.Stress contours for contact simulation with applied/boundary load of 100 N.

B. Effect of Load for Contact Behavior on Ball Bearing

The elastic model was studied in the previous section, while the actual case of what occurs to a ball bearing can be explained more accurately using an elasto-plastic model. Contact simulations for the elasto-plastic model were performed to study the stress distribution and maximum contact pressure on a ball bearing. Boundary loads of 100 N, 200 N, 400 N, 600 N, and 800 N were used for the contact simulations on the ball bearing by taking into account the effect of elasto-plastic deformation. The maximum contact pressure obtained through the simulations for loads of 100 N, 200 N, 400 N, 600 N, and 800 N was 976 MPa, 1048 MPa, 1181 MPa, 1807 MPa and 1980 MPa, respectively. The maximum contact pressure obtained from the analytical calculations was 1800 MPa, 2266 MPa, 2853 MPa, 3266 MPa and 3595 MPa for boundary loads of 100 N, 200 N, 400 N, 600 N, and 800 N, respectively. The graph in Fig. 7 shows the maximum contact pressure vs. the boundary load for the simulations and analytical calculations. The results obtained from the analytical calculations were much higher than the results obtained through the simulations. Hertz's theory was used to obtain the results of the analytical calculations and for the elastic model alone, while the simulations that were carried out took into consideration the effect of elasto-plastic deformation. According to the results obtained by both methods, the maximum contact pressure increased when the boundary load increased. Fig. 8 shows the stress contours of the contact analysis for the elasto-plastic deformation. The stress distribution for the elasto-plastic model was different from that of the elastic model. The stress distribution for the elasto-plastic model was also elliptical, but the maximum von Mises stress occurred from the surface to the centre of the ball and inner ring. The stress distribution for the elastic model was elliptical in shape, and the maximum von Mises stress occurred at the centre of the ball bearing, as can be seen in Fig. 9. The ball was displaced by more than 10% of 3 mm (thickness of the inner ring) when the boundary load reached 800 N. The ball bearing material displayed elastic behaviour when the applied boundary load was less than 400 N, but displayed plastic behaviour when the applied boundary load exceeded 600 N, as shown in Fig. 8. When a boundary load of 600 N was applied, there was a change to a very high displacement.

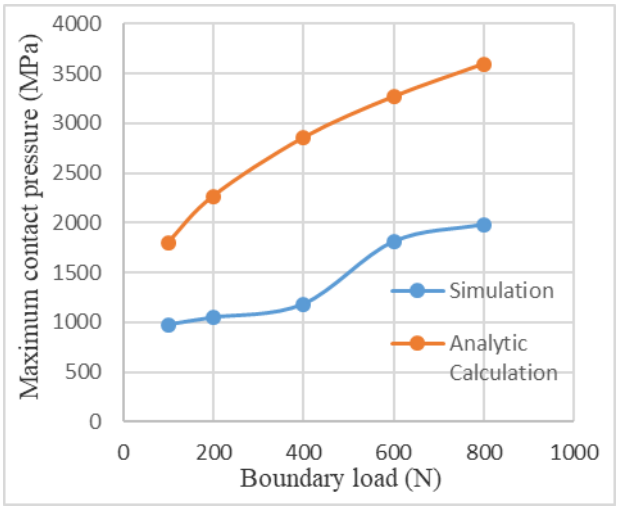

Fig. 7.Graph of Maximum contact pressure vs applied/Boundary load.

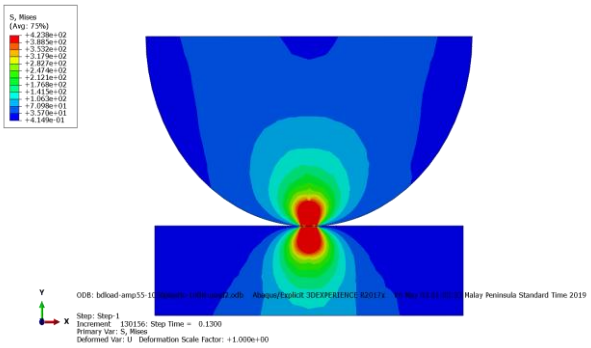

Fig. 8.Stress contours of contact analysis for elasto-plastic deformation with a boundary load of 100 N.

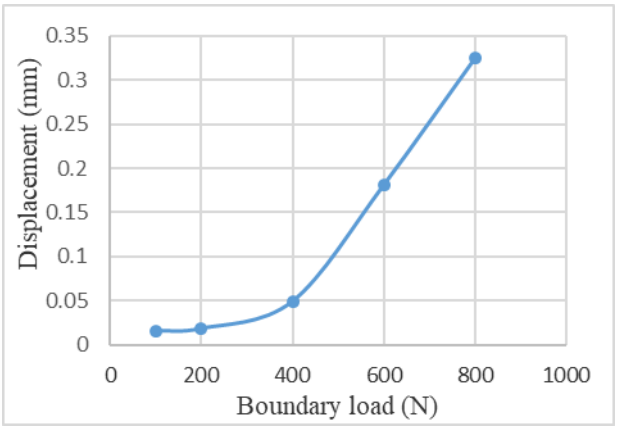

Fig. 9.Graph of Displacement vs. Boundary load.

C. Effect of Plasticity for Contact Behavior on Ball Bearing

Most finite element simulations are carried out using an elastic modulus alone, while the plastic deformation of the material being studied is often ignored (Zamri et al. 2013; 2015; 2016 [23-25]). In this study, an elastic modulus of 200 GPa, a boundary load of 100 N and amplitude of 55 were used for the simulations. Plastic deformation occurred when the stress on the material exceeded the yield stress. The yield stress and ultimate stress were used to study the linear hardening of the material. The distance between the yield stress and the ultimate stress points was given by the slope, which was used to conduct the contact simulations. Fig. 10 shows the loading and unloading behaviour of the linear hardening model. The gradient, E_2, between both the elastic stress and ultimate stress points was entered into the ABAQUS software as the plasticity of the material. E_2 values of 550 MPa, 1050 MPa, 1550 MPa and 2050 MPa were used for the contact simulations on the elasto-plastic model. The equivalent maximum plastic strain for each value of E_2 can be seen in Fig. 11. As the E_2 value increased, the equivalent maximum plastic strain decreased. The equivalent maximum plastic strain decreased with an increase in E_2 because an increase in E_2 indicated a rise in the gradient between both the yield stress and ultimate stress points. This increase caused the plastic strain to drop and the elastic strain to rise. The equivalent plastic strain contours for the contact simulation with a boundary load of 100 N can be seen in Fig. 12. Fig. 13 shows a comparison of the stress distribution between 100 N and 800 N for different values of E_2. The maximum von Mises stress was 420 MPa, while E_2 was 550 MPa and the load was 100 N. The maximum von Mises stress for the simulations with E_2 values of 1050 MPa, 1550 MPa and 2050 MPa and a load of 100 N was 424 MPa, 428 MPa, and 431 MPa, respectively. This showed that the maximum von Mises stress increased with an increase in the value of E_2 in the contact simulations with a load of 100 N. The maximum von Mises stress for the contact simulations using all the values of E_2 and a boundary load of 800 N was 520 MPa. With increasing values of E_2, the area that experienced the maximum von Mises stress increased, as shown in Fig. 13. The maximum von Mises stress was propagated to the material of the ball and inner ring of the ball bearing. In addition, with different values of E_2, the time when the material started to yield also differed. The time when the material started to yield for E_2 values of 550 MPa and 1050 MPa was 0.0455 s, while for E_2 values of 1550 MPa and 2050 MPa it was 0.052 s. The material with a high E_2 value had a longer yield time. Materials with a high E_2 value are able to last longer before experiencing yield compared to materials with a low E_2 value. Fig. 14 shows the yield times for materials with different E_2 values. Fig. 15 shows the time steps for loads of 100 N and 800 N with E_2 of 1050 MPa. The yield time for the ball bearing was 0.0195 s for a boundary load of 800 N, while the yield time for the ball bearing material was 0.0455 s for a boundary load of 100 N. Since the boundary load of 100 N was a load that did not cause the material to undergo ultimate stress, elliptical stress contours were obtained. At 0.0715 s for a boundary load of 800 N, the shapes of the stress contours changed and were no longer elliptical. As the time increased, the contours became as at 0.13 s, as shown in Fig. 15.

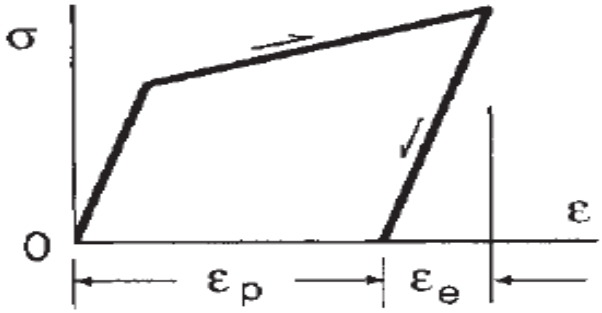

Fig. 10.Loading and unloading behaviour of linear hardening model [3].

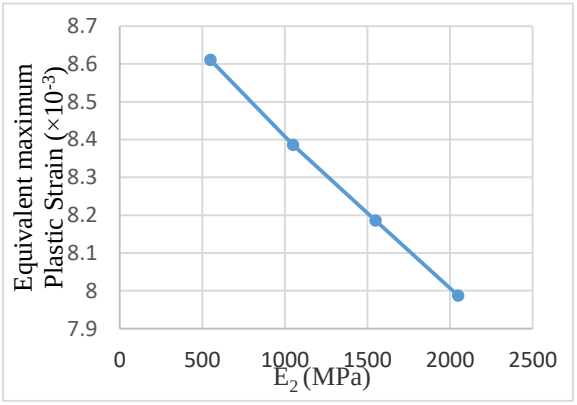

Fig. 11.Graph of Equivalent maximum plastic strain vs. E2.

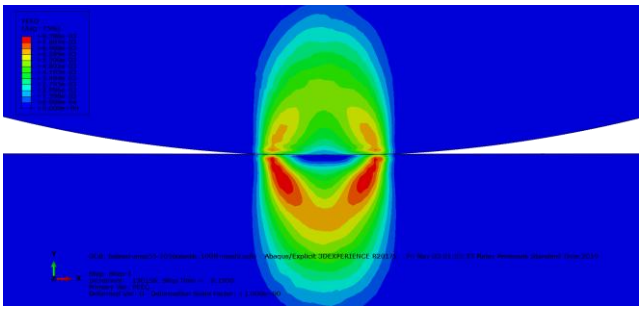

Fig. 12.Equivalent plastic strain for contact simulation with E2 = 1050 MPa.

E_2 (MPa)	Stress distribution (100 N)	Stress distribution (800 N)
550 $VM_{max100N}$ = 420 MPa $VM_{max800N}$ = 520 MPa	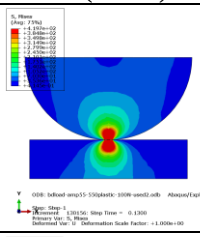	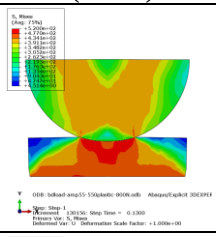
1050 $VM_{max100N}$ = 423 MPa $VM_{max800N}$ = 520 MPa	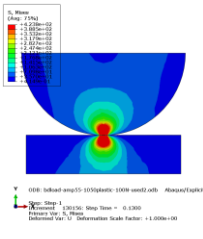	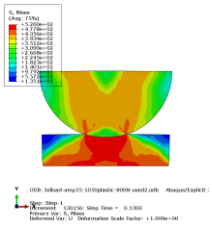
1550 $VM_{max100N}$ = 427 MPa $VM_{max800N}$ = 520 MPa	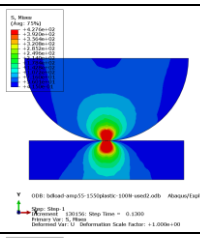	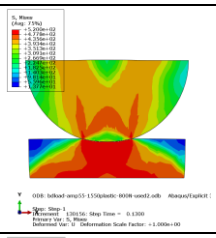
2050 $VM_{max100N}$ = 431 MPa $VM_{max800N}$ = 520 MPa	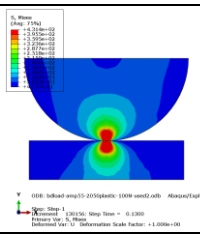	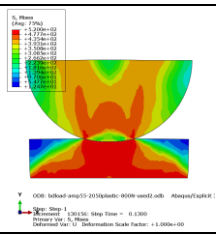

Fig. 13.Comparison of stress distribution between loads of 100 N and 800 N for different values of E2.

E_2 (MPa)	Time (s)	Stress distribution (100 N)
550 $VM_{max100N}$ = 416 MPa	0.0455	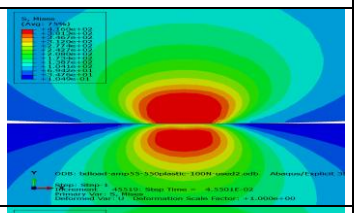
1050 $VM_{max100N}$ = 417 MPa	0.0455	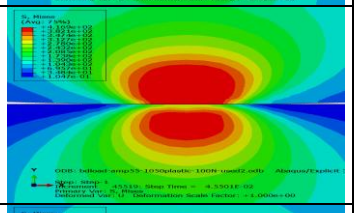
1550 $VM_{max100N}$ = 418 MPa	0.052	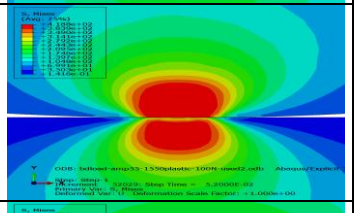
2050 $VM_{max100N}$ = 419 MPa	0.052	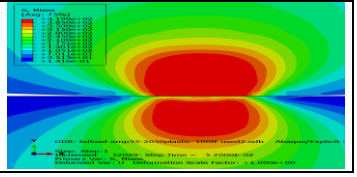

Fig. 14.Time when material begins to yield for different values of E2.

Time (s)	Stress distribution (100 N)	Stress distribution (800 N)
0 $VM_{max100N}$ = 0 MPa $VM_{max800N}$ = 0 MPa	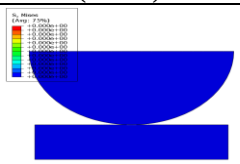	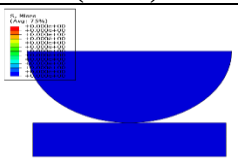
0.0325 $VM_{max100N}$ = 399 MPa $VM_{max800N}$ = 421 MPa	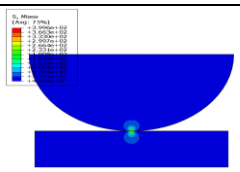	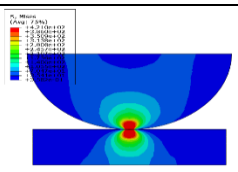
0.0650 $VM_{max100N}$ = 418 MPa $VM_{max800N}$ = 470 MPa	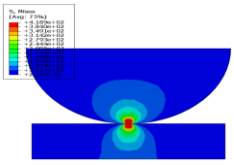	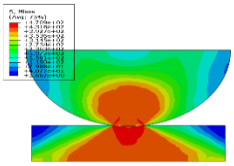
0.0975 $VM_{max100N}$ = 422 MPa $VM_{max800N}$ = 520 MPa	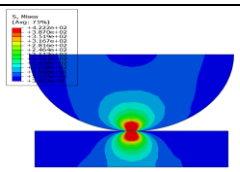	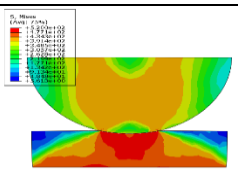
0.1300 $VM_{max100N}$ = 423 MPa $VM_{max800N}$ = 520 MPa	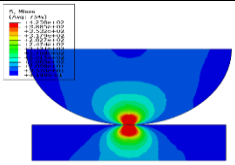	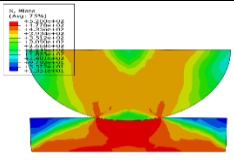

Fig. 15. Time steps for loads of 100 N and 800 N with E2 of 1050 MPa.

V. CONCLUSION

The contact simulation was performed by using finite element software of ABAQUS to study the ball bearing type of 6309 DGBB. Several methods were used to verify the elasto-plastic contact model used for contact simulation. A mesh convergence study was conducted to ensure an accurate results obtained from the simulations.

The simulation result started to converge when the number of element was 9522.

The other method to verify the contact analysis is to use amplitude. An amplitude of 55 was used to reflect the actual case of contact behaviour on ball bearing. A maximum contact pressure of 1751 MPa was obtained through the finite element simulation.

This result was then used to compare with result obtained from the other journal. The maximum contact pressure obtained from Londhe et al. 2018 [7], was 1785 MPa and the percentage difference was only 1.90 %.

As the percentage difference was lower than 5 %, this model was validated and could be used to perform other analysis to achieve the objective of this study.

The effect of a load on the elasto-plastic deformation on contact was studied using loads of 100 N, 200 N, 400 N, 600 N and 800 N.

The maximum contact pressure obtained through the simulations for the elasto-plastic model was much lower than the maximum contact pressure obtained from the Hertz theory because plasticity was taken into account in these simulations, while the Hertz theory only focused on the elastic model. The displacement of the ball bearing exceeded 10 % from 3 mm (thickness of the inner ring) when the boundary load reached 800 N. The effect of various values of E_2 on the contact pressure was also studied. Equivalent maximum plastic strains of 8.610×10^{-3}, 8.386×10^{-3}, 8.185×10^{-3} and 7.987×10^{-3} were obtained for E_2 values of 550 MPa, 1050 MPa, 1550 MPa, and 2050 MPa, respectively. The yield time for the ball bearing for E_2 values of 550 MPa and 1050 MPa was 0.0455 s, while for 1550 MPa and 2050 MPa, it was 0.052 s. The stress distribution and elasto-plastic deformation were studied and obtained for the contact analysis of the ball bearing.

Various suggestions can be made for improving this study. This study only focused on the ball and inner ring of the ball bearing. A 2-dimensional model was used for the contact analysis. The contact analysis can be performed by using a coating on the ball and inner ring. Most ball bearings in industrial applications use a coating to extend the life of the ball bearings as well as to save on maintenance costs. Ball bearings that use grease as a lubricant require regular maintenance, while coated ball bearings do not require maintenance. In addition, this study only conducted simulations on one part of the ball bearing. Another suggestion is that the simulations be conducted using the full model of a ball bearing and not just a part of it. A 3-dimensional model can be used to analyse the contact between the ball and the inner ring as such a model will be almost similar to the actual ball bearing. A wear analysis can also be performed to study the spalling of the ball bearing material. Cyclic loading with sliding and rolling motions can be carried out to study the spalls on the ball bearing after a certain number of cycles.

VI. ACKNOWLEDGEMENT

The authors would like to thank the Malaysia research foundation - Geran Universiti Penyelidikan: GUP-2018-149: for funding this work. This project also has received funding from the European Unions's Horizon 2020 research and innovation programme under the Marie Sklodowska-Curie grant agreement No 730888.

REFERENCES

1. ABAQUS. 2017. Simulia user assistance 2017. United State: Dessault Systemes Simulia Corporation.
2. Arakere, N. K. 2016. Gigacycle rolling contact fatigue of bearing steels: A review. *International Journal of Fatigue* 93(June): 238–249.
3. Dowling, N. E. 2013. Mechanical Behavior of Materials. 4th Ed. Pearson: United States.
4. Guo, Y. & Parker, R. G. 2012. Stiffness matrix calculation of rolling element bearings using a finite element/contact mechanics model. *Mechanism and Machine Theory* 51: 32–45.
5. Komba, E. H., Massi, F., Bouscharain, N., Le Jeune, G., Berthier, Y. & Maheo, Y. 2016. Experimental damage analysis in high loaded oscillating bearings. *Tribology International* 102: 507–515.
6. Li, S. 2018. A mathematical model and numeric method for contact analysis of rolling bearings. *Mechanism and Machine Theory* 119: 61–73.
7. Londhe, N. D., Arakere, N. K. & Subhash, G. 2018. Extended Hertz Theory of Contact Mechanics for Case-Hardened Steels With Implications for Bearing Fatigue Life. *Journal of Tribology* 140(2): 1-11.
8. Massi, F., Bouscharain, N., Milana, S., Le Jeune, G., Maheo, Y. & Berthier, Y. 2014. Degradation of high loaded oscillating bearings: Numerical analysis and comparison with experimental observations. *Wear* 317(1–2): 141–152.
9. Mishra, D., & Soni, P. K. 2018. Effect of Amplitude at some bearing speeds and radial loads on Defective Deep Groove Ball Bearing. *International Research Joutnal of Engineering and Technology* 5(5): 3621–3626.
10. Qiu, M., Chen, L., Li, Y. & Yan, J. 2017. Bearing Tribology. 1st Ed. Beijing: Springer.
11. Rezaei, A., Van Paepegem, W., De Baets, P., Ost, W. & Degrieck, J. 2012. Adaptive finite element simulation of wear evolution in radial sliding bearings. *Wear* 296(1–2): 660–671.
12. Shan, X., Xie, T., Chen, W. & Wang, L. 2009. Modeling and simulation on the contact deformation distribution in a wire race ball bearing. *2009 IEEE International Conference on Robotics and Biomimetics, ROBIO 2009* (1): 2211–2214.
13. Shan, X., Yuan, J., Xie, T. & Qi, H. 2009. A new approach for determining the contact indentation of the wire race ball bearing in a three-axis simulating rotary table. *2009 IEEE International Conference on Mechatronics and Automation, ICMA 2009* 3916–3920.
14. SKF: Deep groove ball bearings. (n.d.). https://www.skf.com/us/products/bearings-units-housings/ball-bearings/deep-grove-ball-bearings/deep-groove-ball-bearings/index.html?designtion=6309 [29 May 2019]
15. Stachowiak, G. W. & Batchelor, A. W. 2005. Engineering tribology. 3rd Ed. Elsevier: United States.
16. Tang, Z. & Sun, J. 2011. The contact analysis for deep groove ball bearing based on ANSYS. *Procedia Engineering* 23: 423–428.
17. Tonazzi, D., Komba, E. H., Massi, F., Le Jeune, G., Coudert, J. B., Maheo, Y. & Berthier, Y. 2017. Numerical analysis of contact stress and strain distributions for greased and ungreased high loaded oscillating bearings. *Wear* 376–377: 1164–1175.
18. Vieillard, C., Kadin, Y., Morales-Espejel, G. E. & Gabelli, A. 2016. An experimental and theoretical study of surface rolling contact fatigue damage progression in hybrid bearings with artificial dents. *Wear* 364–365: 211–223.
19. Wakabayashi, N., Murakmi, N. & Takaichi, A. 2018. Current Applications of Finite Element Methods in Dentistry. *Handbook of Mechanics of Materials* 1-28.
20. Wang, C., Yu, W. & Ren, C. 2011. An Accurate Method for Calculating the Contact SubsurfaceStress Field of Hybrid Ceramic Ball Bearing 175: 215–218. doi:10.4028/www.scientific.net/SSP.175.215.
21. Yang, L., Deng, S. & Li, H. xing. 2016. Numerical analysis of loaded stress and central displacement of deep groove ball bearing. *Journal of Central South University* 23(10): 2542–2549.
22. You, H., Chun-xi, Z. & Wu-xing, L. 2012. Contact Analysis on Large Negative Clearance Four-point Contact Ball Bearing 37(Cems): 174–178.
23. Zamri, W.F.H., Kosasih, P.B., Tieu, A.K., Zhu, H. and Zhu, Q., 2013. Finite element modeling of the nanoindentation of layers of porous oxide on high speed steel. *steel research international*, *84*(12), pp.1309-1319.
24. Zamri, W.F.H.W., Kosasih, B., Tieu, K., Ghopa, W.A.W., Din, M.F.M., Aziz, A.M. and Hassan, S.F., 2016. A simulation of friction behavior on oxidised high speed steel (HSS) work rolls. ARPN Journal of Engineering and Applied Sciences, 11(12), pp.7394-7400.
25. Zamri, W.F.H.W., Kosasih, B., Tieu, K., Ghopa, W.A.W., Din, M.F.M., Aziz, A.M. and Hassan, S.F., 2015. Effect of Carbide Particles on the Behaviour of the Oxide Layer. Research Journal of Applied Sciences, Engineering and Technology, 11(8), pp.910-920.
26. Zhou, X., Li, D. & Yu, R. 2011. Finite element analysis of the contact problem for a wire race ball bearing used in a rotating platform. *Proceedings - 3rd International Conferencen on Measuring Technology and Mechatronics Automation, ICMTMA 2011* 2: 221–224.

AUTHORS PROFILE

Leong Chee Yau, is a research assistant at Universiti Kebangsaan Malaysia (UKM). He obtained his degree at Universiti Kebangsaan Malaysia (UKM). His research interests include, surface engineering, contact and wear modelling.

Wan Fathul Hakim Bin Wan Zamri, is a senior lecturer at Universiti Kebangsaan Malaysia (UKM). He obtained his bachelor at Universiti Kebangsaan Malaysia (UKM) and PhD at University of Wollongong, Australia. His areas of expertise include computational tribology and wear of materials.

Intan Fadhlina Binti Mohamed, is a senior lecturer at Universiti Kebangsaan Malaysia (UKM). She obtained her bachelor and master at Universiti Kebangsaan Malaysia while PhD at KYUSHU University. Her areas of expertise are severe plastic deformation, nanostructured materials and precipitation hardening.

Ahmad Kamal Ariffin Mohd Ihsan, is a professor at Universiti Kebangsaan Malaysia (UKM). He obtained his bachelor at Universiti Kebangsaan Malaysia (UKM) and PhD at University of Wales. His areas of expertise include computational methods, fracture mechanics, friction, corrosion, finite element/discrete element and parallels computations.

Muhammad Faiz Md Din, is a lecturer at Universiti Pertahanan Nasional Malaysia. He obtained his bachelor and master at University of Huddersfield while PhD at University of Wollongong, Australia. His expertise are superconductor, semiconductor, magnetism material, condenser matter, advance material application, X- ray diffraction and neutron diffraction.